A Study on Observation and Growth Behavior of Small Surface Cracks by Remote Measurement System

Seung Hoon Nahm*, Hae Moo Lee* and Chang Min Suh**

(Received September 13, 1995)

A new experimental system using remote measurement system (RMS) and image processing technique was applied for studying the growth behavior of small surface fatigue cracks in 1Cr-1Mo-0.25V steel at room temperature. The system includes a long distance focusing microscope, a CCD camera, a light source, a 3-axis controller, a monitor, a personal computer and a data translation card. The measurement error of the system appeared to be 0.8%. It is possible for this system to measure down to 30 μm of surface fatigue crack length. The length of surface fatigue crack could be successfully measured by the RMS during testing as well as after the test. The growth rate of small cracks on smooth specimens was represented in terms of stress intensity factor and J-integral. At equivalent elastic stress intensity factor levels, the growth rate of small surface cracks was not consistent and faster than that of long crack of CT specimen.

Key Words: Surface Fatigue Crack, Small Crack, 1Cr-1Mo-0.25V Steel, Remote Measurement System, Stress Intensity Factor, J-Integral, Image Processing Technique

1. Introduction

The size of pre-existing flaw like an inclusion in materials is getting smaller due to the improvement of manufacturing process of materials. Experimental studies on the growth behavior of small crack are recently concerned because the growth life of small crack initiated from pre-existing flaws takes large portion of the total fatigue life. (Howland, 1986 ; Kitagawa, 1979 ; Suh, 1994) Many researchers (Kitagawa, 1979 ; Saxena, 1985 ; Lankford, 1986) are making clear the difference between long crack growth behavior and small crack one. As a result, advanced experimental methods to study the growth behavior of small surface crack are required.

Replica method (Suh, 1994 ; Swain, 1992) is widely used to measure growth rates of small surface cracks, and has advantages in respect of simplicity and easiness. However, much time and more man power are required because of the periodical replication. To be worse, the replication is not possible at elevated temperature in case of high temperature test. The SEM could be the best for the precise method, but specially designed equipments are required for its usage. (Davidson, 1992) Therefore, the development of a new measuring system is required for observing the growth behavior of surface fatigue crack at elevated temperature.

Among many kinds of testing methods, a remote measurement system (RMS) has many advantages in comparison with the methods explained above. Because of that, the RMS accompanied with an image processing technique was introduced in this study to observe the behavior of small surface fatigue crack which was initiated and grown in smooth surface of 1Cr-1Mo-0.25V rotor steel. The characteristics of surface crack growth measured by RMS were analysed and estimated using stress intensity factor or J-integral. In addition, the growth behaviors of small crack were compared with those of long crack.

* Korea Research Institute of Standards and Science, P. O. Box 102, Yusong, Taejon, 305-600, Korea

** Kyungpook National University, 1370 Sankyuk-dong, Pook-ku, Taegu, 702-701, Korea

2. Testing Method

2.1 Experimental setup using remote measurement system

The RMS was composed of a set of a long distance focusing microscope, a light source, a three-axis controller, a monitor, a digital indicator, a CCD camera, a personal computer, a data translation card (image card), etc.. Figure 1 is the schematic diagram of the system. The image displayed in the monitor was obtained with the long distance focusing microscope and a CCD camera. The focusing distance of the microscope was approximately 840 mm, and magnification range was 80 ~ 480 times depending on the combination of various kinds of lens. A unit cell size of the CCD camera was $8.4\mu m \times 9.8\mu m$. Thus, each individual pixel of input image indicates $0.7\mu m$ in actuality. As a result, the crack only larger than $30\mu m$ could be distinguished by this system.

In this study, crack length could be measured not only during the cycling but also after the testing, because the image of a crack was stored in the personal computer by using image processing technique (data translation : DT 3851). In case of storing the image of a crack in personal computer by using DT 3851, the required capacity of memory for one image frame was about 0.3 Mbyte. A large memory capacity was needed for recording the behavior of fatigue crack initiated naturally in a specimen. For recording the fatigue crack, the image of the specimen surface could be stored in the video tape. During the display of the video tape, a chosen region which had a crack could be analyzed in personal computer by using DT 3851 and then the length of crack was measured. However the quality of image stored in the video tape was not so good in comparison with the direct image on personal computer through DT 3851.

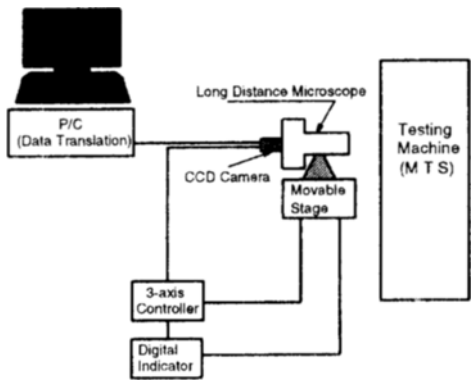

Fig. 1 Schematic diagram of experimental setup using the remote measurement system.

2.2 Specimens

The test material was a 1Cr-1Mo-0.25V steel which is widely used for turbine rotor material, and the chemical compositions are shown in Table 1. The microstructure of the material consists of fine pearlite, ferrite and sorbite, and the average grain size measured by a line-intercept method was about $25\mu m$. Tensile specimens were machined to a 6.35 mm diameter and 41.9 mm long. The longitudinal direction of tensile specimen was cut along circumferential direction of cylindrical material as shown in Fig. 2. Tensile tests were performed at a displacement rate of 10 mm/min according to ASTM E 8(1992) with a closed loop servohydraulic testing machine. Hardness tests were conducted with micro-Vickers hardness tester. Mechanical properties of the specimen at room temperature are shown in Table 2.

2.3 Methods of fatigue testing

Compact tension (CT) specimens with 6.7 mm in thickness were machined from cylindrical raw material like Fig. 2. The crack plane orientation of CT specimens was the same with the code C-R which is designated in ASTM E647(1992), where C is circumferential direction and R is radial

Table 1 Chemical composition of 1Cr-1Mo-0.25V steel (Wt, %).

C	Si	Mn	P	S	Ni	Cr	Mo	V	As	Sn	Sb
0.31	0.23	0.76	0.006	0.001	0.36	1.11	1.32	0.27	0.006	0.005	0.001

Table 2 Mechanical properties of 1Cr-1Mo-0.25V steel.

Yield Stress (0.2%) (MPa)	Tensile Strength (MPa)	Elongation (%)	Reduction of Area (%)	Hardness (Hv)
665.2	823.1	18.8	59.4	266

direction. The fatigue test of CT specimens was performed in an ambient atmosphere at a frequency of 10 Hz with a load ratio of R=0.05 under sinusoidal waveshapes according to ASTM E 647.(1992)

The smooth specimens were prepared as shown in Fig. 2 in order to observe the propagation of small surface fatigue crack, and the direction of surface crack growth was in accordance with the longitudinal direction of cylindrical material. The dimensions of the smooth specimen are shown in Fig. 3. This was specially designed as an semi-hourglass type for examining the initiation and growth of small surface crack near the center portion of it.

The fatigue test of the smooth specimen was performed in an ambient atmosphere at a frequency of 10 Hz with a load ratio of R=0.05 under sinusoidal waveshapes. The stress levels applied to smooth specimen were 441, 491, 544 and 637 MPa. The crack length was measured at the 80% of maximum fatigue load while the cyclic loading was interrupted. And the image of crack was stored in personal computer with image processing technique. In addition, the surface of specimen was replicated using a cellulose acetate sheet, 0.04 mm thick.

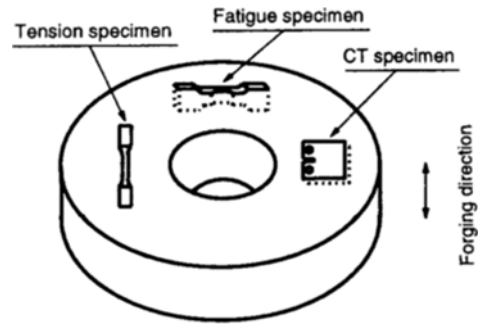

Fig. 2 Specimen orientation taken from a turbine rotor steel.

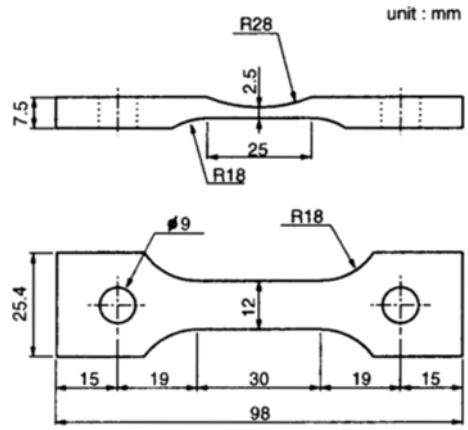

Fig. 3 Geometry of surface fatigue specimen.

3. Results and Discussion

3.1 Measuring capability on RMS

3.1.1 Measuring accuracy on RMS

RMS (remote measurement system) was calibrated for evaluating the measurement of accuracy. Before the test, a light source was set up with proper intensity and angle. After that, RMS was set up to be horizontal with 200 mm scale. The accuracy of RMS was confirmed by comparing a scale of the ruler with the value read from the digital indicator. The mean value measured by RMS was 39.68 mm for the four times measurement of 40 mm of the ruler. Therefore, the error between the real length and the measuring value was -0.8%.

The accuracy of various measuring methods was evaluated on the small defect made by electro-discharge machining (EDM) in a specimen. Table 3 shows the values measured by scanning electron microscope, optical microscope, RMS and replica. The value by scanning electron microscope was the most accurate among the values obtained by the four kinds of measurement

Table 3 Comparison of accuracy among the 4 kinds of measurement methods.

SEM	Microscope	RMS	Replica
180μm	176μm	179μm	171μm

methods. According to the results of the measurement for an artificial defect(diameter : 180μm, maximum depth : 10μm), RMS, optical microscope and scanning electron microscope were almost the same in the measurement capability. The measurement accuracy of replica method lagged behind that of other methods, and the measurement error of replica method was -5%. Therefore, the RMS adopted in this test was more useful and accurate for measuring the crack length than replica method. In addition, a large number of data could be obtained quickly in real time and could be measured through the personal computer.

3.1.2 Advantages and disadvantages of RMS

In the aspects of RMS, several advantages and disadvantages are as follows:

〈 Advantages 〉

(1) Fatigue crack initiated at smooth surface can be measured and its image can be stored directly using the RMS.

(2) This system provides the records of crack initiation and growth behavior with the aid of a micro-computer.

(3) A large number of data may be obtained quickly, and the measurement precision of surface crack length is good. The length of surface fatigue crack could be measured during testing as well as after the test.

(4) This system could be applicable to measure the small crack behavior at elevated temperature and in vacuum or inert gas.

〈 Disadvantages 〉

(1) The crack depth can not be measured directly by this system because only the surface crack length can be measured.

(2) Cracks smaller than 30μm can not be measured in real time.

(3) To record the images of cracks at initiation and growth on smooth specimen, a large computer memory is necessary.

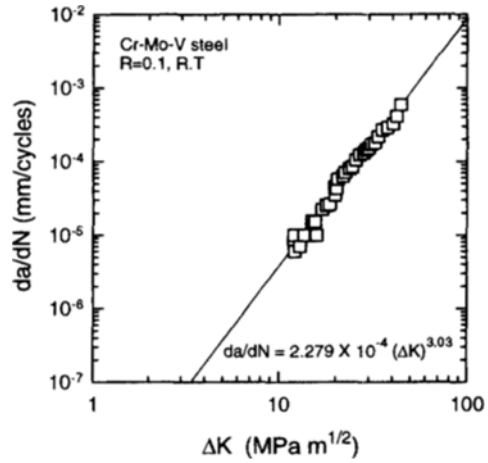

Fig. 4 Dependence of long crack growth rate of CT specimen upon stress intensity factor range.

3.2 Fatigue crack growth rate at the CT specimen.

Figure 4 shows the data of long crack growth rate in CT specimens. Stress intensity factor range, K, was calculated using the equation from the ASTM E 647(1992). Crack growth rates were represented as Eq.(1). The exponent of fatigue crack growth rate was m=3.40, and the constant was C=1.4791×10^{-9}.

$$\frac{da}{dN}=1.4791\times10^{-9}(\Delta K)^{3.40} \quad (1)$$

3.3 The initiation and growth behavior of a small crack

Figure 5(a) shows the surface crack of the specimen tested at 441 MPa by scanning electron microscope (SEM). Figure 5(a) indicates that the major crack grew almost symmetrically from the initiation site. Its fracture surface is shown in Fig. 5(b). An artificial defect (marked as D in Fig. 5(a)) of 180μm in diameter and 10μm in depth was made by an electro discharging machine (EDM) at the central portion of the specimen in order to easily observe the initiation

and growth behavior of a small crack. The crack initiated at this artificial defect was measured as 200μm at the cycle of 250,000 and 304μm at the cycle of 260,000. But a small fatigue crack was initiated from an intrinsic defect (marked as A in Fig. 5(a)) of material, even though the size of the artificial defect was bigger than that of the intrinsic defect. This small crack initiated from the intrinsic defect A was grown to a major crack which governed the fatigue life of the specimen.

Figure 5(b) shows a typical fatigue fracture surface of plate specimen. Figure 5(c) is a magnified view of fracture surface near the crack initiation site marked as A in Fig. 5(b). Figure 5(c) shows a lot of small inclusions at SEM photograph of fracture surface. Figure 5(c) implies that the major crack was initiated at one of these inclusions. Figure 5(d) shows the major chemical compositions of the inclusion in Fig. 5(c). The compositions of inclusions were quite different from those of matrix as shown in Table 4. About 71% of the composition of the inclusion is Al. The major element of the matrix is Fe, being 93%. This means that the inclusions are mainly aluminium oxide.

Figure 6 shows the fracture surface of the specimen tested at 637 MPa. Inclusions were distributed in a band at an angle of about 30 degrees with the surface. The major elements of these inclusions were similar to those in Fig. 5(c). The major crack also appeared to be initiated at these inclusions.

Table 4 Comparision of chemical composition of an inclusion and matrix at initiation area of a major crack.

Component	Inclusion (Wt, %)	Matrix (Wt, %)
Al	70.8	-
Ca	17.3	-
Fe	6.9	93.5
P	4.0	-
Ti	1.1	-
Mn	-	3.2
Cr	-	2.3
Mo	-	1.0
Si	-	0.1

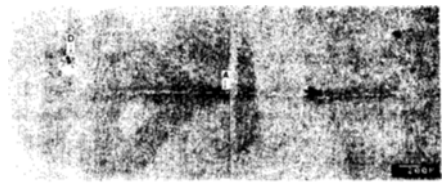

(a) Crack propagation behavior.

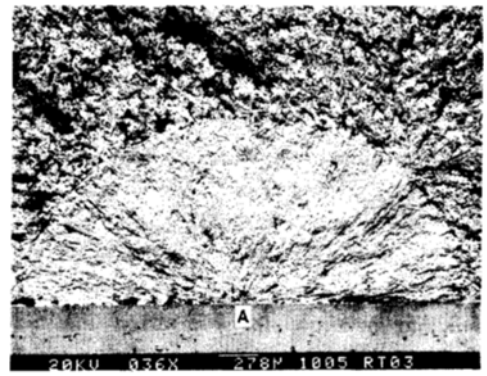

(b) View of fracture surface.

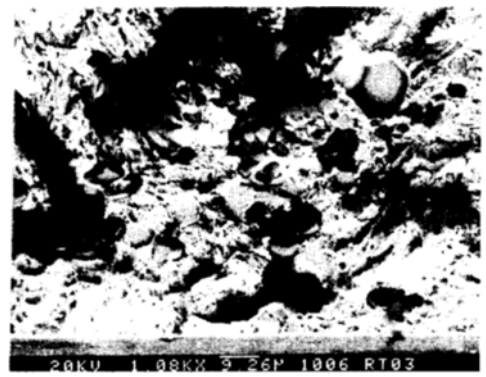

(c) Magnified view of fracture surface near crack initiation site.

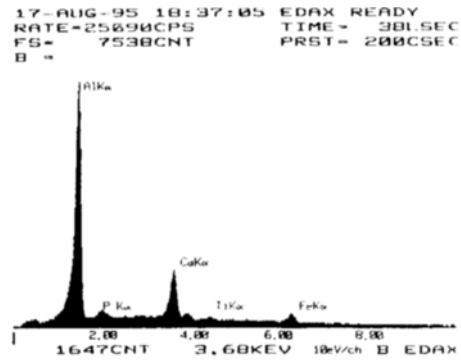

(d) EDX analysis for the inclusion in Fig. 5(c)

Fig. 5 Crack propagation behavior of a smooth specimen tested at 441 MPa at room temperature. A indicates crack initiation site.

Fig. 6 View of fracture surface tested at 637 MPa.

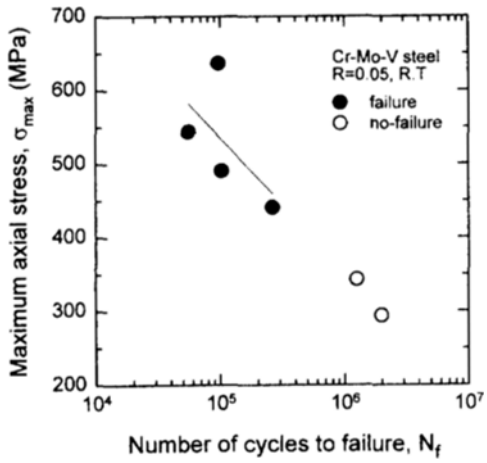

Fig. 7 The realtionship between the maximun axial stress, σ_{max} and the number of cycle to failure, N_f.

3.4 The characteristics of S-N curve

Figure 7 shows the relationship between the maximum axial stress and the number of cycle to failure. Failure means that the length of crack reached to about 4.5 mm. Solid and hollow symbols represent the specimens of failure and no -failure, respectively. If a crack propagates larger than this size, the unstable fracture takes place. In order to investigate the aspect ratio, the test was stopped to avoid the unstable fracture.

The number of cycles to failure at 637 MPa is much larger than that at 544 MPa, which might be because of the inclusions gathered below the surface. Failure did not take place until 1.26×10^6 cycles and 2.0×10^6 cycles at 343 MPa and 294 MPa, respectively. Any cracks were not found during 1.26×10^6 cycles at 343 MPa. Therefore, the fatigue limit may be a little higher than 343 MPa.

3.5 The relationship between the fatigue crack length and the cycle ratio

Figure 8 is the plot of surface crack length versus cycle ratio. The data lie within a relatively narrow band for the four different stress levels. This aspect shows the same trend as the other reports.(Kitagawa, 1979 ; Suh, 1987a ; Suh, 1984) It shows that more than 80% of the total life is consumed for the crack to grow up to 800μm. Cracks larger than 800μm grew fast and eventually led to fracture.

This result was consistent with the results of other studies(Suh, 1987a ; Suh, 1984 ; Suh, 1987 b) that the cracks are rapidly growing above nearly 80% of the total life. This means that the crack growth could be inspected and controlled because the crack was gradually growing under 80% of fracture life, but it would not be easy to find it because of its very small size. It will be difficult to control crack growth over 80% of fracture life because of its rapidity. The result shows that understanding of the small crack growth on the smooth specimen is more important for the life prediction than that of the large crack growth.

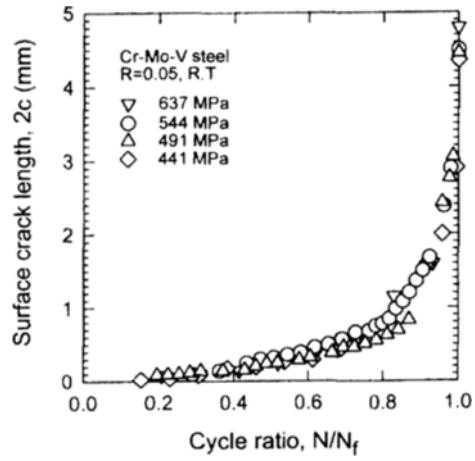

Fig. 8 The relationship between surface crack length, 2c and cycle ratio, N/N_f.

3.6 Variation of the aspect ratio

The crack length in depth-direction as well as on the surface should be considered to understand the growth characteristics of a small crack which was initiated naturally. However, the aspect ratio (a/c) on the crack growth could not be measured directly by using the RMS or the replication method. Where a is crack depth and c is surface crack length.

In order to measure the aspect ratio, several fatigued specimens with different surface crack lengths were fractured under monotonic loading at low temperature. The crack lengths on the surface and in depth-direction from the fractured surface were measured with an optical microscope.

Figure 9 shows the variation of aspect ratio (a/c) according to the ratio of crack depth to specimen thickness (a/t). The initial aspect ratio of the order of 1.3 is for incipient surface cracks initiated at inclusions. The aspect ratio was decreasing until a/t became 0.6 and it was converged into 0.84. This result was in a good agreement with the data of Suh et al. .(Suh, 1987a ; Suh, 1984) The relationship of aspect ratio could be expressed as Eq.(2).

$$a/c = 1.2445 - 1.8451(a/t) + 3.0591(a/t)^2 - 1.6773(a/t)^3 \quad (2)$$

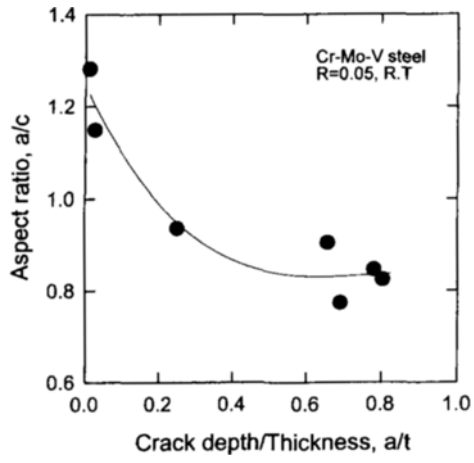

Fig. 9 The variations of aspect ratio.

3.7 Dependence of crack growth rate on stress intensity factor range

The data of surface crack growth rates from the smooth specimen were expressed in terms of stress intensity factor range in order to compare with those of the CT specimen. The equation suggested by Newman-Raju (1983) was used to calculate the stress intensity factor range.

Figure 10 shows the relationship between the surface crack growth rate (dc/dN) and the stress intensity factor range (ΔKc). In this figure, the solid line indicates the regression line of the CT specimen as shown in Fig. 4. In Fig. 10, the behavior of small surface crack growth on the smooth specimen was compared with that of long crack growth in the CT specimen. As shown in Fig. 10, the small surface crack growth rates were very irregular below the stress intensity factor range of 15 MPa$\sqrt{m}$ and were located above the regression line of the CT specimen. From these data, we could find that small surface crack growth rates were faster than those of long crack at equivalent stress intensity factor range. But the crack growth rates of smooth specimen at larger stress intensity factor range than 15 MPa$\sqrt{m}$ were similar to those of the CT specimen. Similar result had been reported by Kitagawa et al. . (1979)

Arrow in Fig. 10 represented the transition

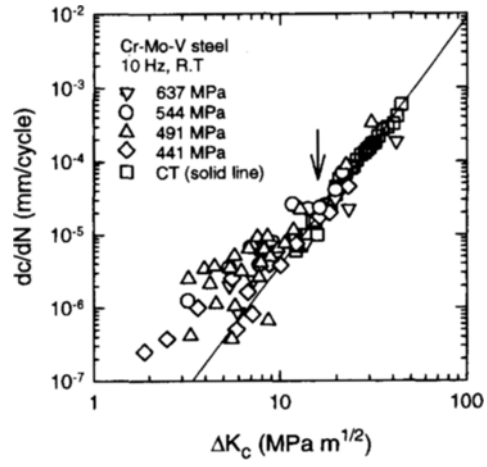

Fig. 10 Dependence of surface crack growth rate upon stress intensity factor range. Solid line indicates the regression line of CT specimen.

point of a small and a large crack, and the transition crack size was equivalent to about 800μm in this experiment. This crack size, 800μm, was about 30 times of the average grain size, 25μm, and this result is in a good agreement with the other results of Nahm et al.(1990) in the turbine blade material.

The small surface crack growth rates in Fig. 10 were very irregular because of the interaction between the local plastic deformation by the high stress level and the effect of grain boundary. (Kitagawa, 1979) Since the small crack growth rates could not be characterized in terms of ΔK, other parameters are necessary for expressing the growth behavior of a small crack.(Kitagawa, 1979 ; Suh, 1992)

3.8 Dependence of crack growth rate on J-integral

J-integral as shown in the Eq.(3) suggested by Hoshide-Socie(Hoshide, 1987) was used to analyze the small crack growth rates in this study. At this time, the length of small crack was modified to consider the plastic zone size.

$$J=\frac{(\sigma\sqrt{\pi a_{eff}})^2}{E}+f(n)\,\sigma\varepsilon_p a$$
$$f(n)=3.85(1-n)/\sqrt{n}+\pi n$$
$$a_{eff}=a+r_y \quad \text{if } \sigma\le\sigma_y(1-a/W)\approx\sigma_y$$
$$=[a_{eff}]_{\sigma=\sigma_y}, \quad \text{if } \sigma>\sigma_y(1-a/W)\approx\sigma_y$$
$$r_y=\frac{1}{2\pi}\left(\frac{1-n}{1+n}\right)\left(\frac{K_I}{\sigma_y}\right)^2 \qquad (3)$$

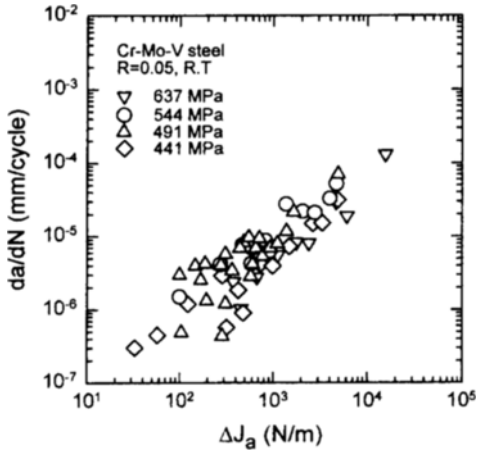

Fig. 11 Dependence of depth crack growth rate upon J-integral range.

where a is a crack depth, a_{eff} is an effective crack length considering the plastic zone, n is a hardening coefficient, W is the specimen width, ε_p is the plastic strain rate, E is an elastic modulus and σ_y is a yield strength. In the above equation, the second term is negligible because applied maximum stress is lower than the yield strength. And a hardening coefficient obtained by experiment is 0.0392.

Figure 11 shows the relationship between the crack depth growth rates and J-integral. Even though the growth rates of small crack were analyzed by J-integral, the tendency of irregularity in propagation like Fig. 10 was also observed in Fig. 11. It also implies that the crack depth growth rates in terms of ΔJ could not be characterized in the two regions, i.e., small crack region ($\Delta J < 2\times10^3$ N/m) and large crack region ($\Delta J > 2\times10^3$ N/m). Therefore, it is confirmed that the J-integral considering the only plastic zone size is not useful as the driving force for small crack growth.

4. Conclusion

The growth behavior of a small crack initiated and propagated on smooth specimen of 1Cr-1Mo-0.25V steel for a turbine rotor material was studied by applying the remote measurement system(RMS) with image processing technique. The experimental results were obtained as follows:

(1) The initiation and growth of a small surface fatigue crack could be observed directly by using the RMS. The crack size could be measured and stored in micro-computer with image processing technique. This method was more convenient than the conventional testing method, and could reduce the testing time. In case of measurement, it was possible for this system to measure down to 30μm of surface fatigue crack length during testing.

(2) When the growth rate of small crack was represented as ΔK, stress intensity factor range, it was not consistent and higher than that of the long crack at equivalent stress intensity factor range. When the crack length was larger than 800μm on smooth specimen, the crack growth

behavior was similar to that of CT specimen. The size of crack for the conversion of a small crack to a long crack on smooth specimen, about 800μm, was almost 30 times of average grain size. J-integral was proven to be not useful for characterizing the behavior of a small crack growth on smooth specimen.

Acknowledgment

The authors thank the Korea Science and Engineering Foundation(KOSEF) for financial support via the research grant project No.951-1009-078-2.

References

Davidson, D. L., 1992, "The Experimental Mechanics of Microcracks," *ASTM STP* 1149, pp. 81~91.

Hoshide, T. and Socie, D. F., 1987, "Mechanics of Mixed Mode Small Fatigue Crack Growth," *Engineering Fracture Mechanics*, Vol. 6, No. 6, pp. 841~850.

Howland, C., Hicks, M. A. and Jeal, R. H., 1986, "The Relevance of Short Crack Behaviour to the Integrity of Major Rotating Aero Engine Component," *Proceedings of 2nd Conference on Small Fatigue Cracks. U. S. A.*, pp. 607~622.

Kitagawa, H., Takahashi, S., Suh, C. M. and Miyashita, S., 1979, "Quantitative Analysis of Fatigue Process — Microcracks and Slip Lines under Cyclic Strains," *ASTM STP* 675, pp. 420~449.

Lankford, J. and Davidson, D. L., 1986, "The Role of Metallurgical Factors in Controlling the Growth of Small Fatigue Cracks," *Proceedings of 2nd Conference on Small Fatigue Cracks. U. S. A.*, pp. 51~71.

Nahm, S. H., Lee, J. J., Huh, Y. H., Jeon, S. B. and Lee, H. M., 1990, "Behavior of Small Crack Growth in Steam Turbine Blade Material," in Korea *J. of the Korean Inst. of Metals*, Vol. 28, No. 10, pp. 881~886.

Newman, J. C. and Raju, I. S., 1983, "Stress Intensity Factor Equations for Cracks in Three-Dimensional Finite Bodies," *ASTM STP* 791, pp. 238~265.

Saxena, A., Wilson, W. K., Roth, L. D. and Liaw, P. K., 1985, "The Behavior of Small Fatigue Cracks at Notches in Corrosive Environments," *International Journal of Fracture*, Vol. 28, pp. 69~82.

Suh, C. M. and Kang, Y. G., 1987a "A Basic Study on Growth Characteritics of the Small Surface Crack in 2.25Cr-1Mo Steel," in Korea, *J. of Ocean Engineering and Technology*, Vol. 1-1, pp. 104~110.

Suh, C. M. and Kim, G. N., 1984, "A Study on the Initiation and Growth Behaviors of Surface Crack in a Type 304 Stainless Steel at Room Temperature," in Korea, *Trans. of KSME*, Vol. 8, No. 3, pp. 195~200.

Suh, C. M., Hwang, N. S. and Park, M. K., 1994, "Fatigue Crack Growth, Coalescence Behavior and Its Simulation on Multi-Surface Cracks," in Korea *Trans.* of *KSME*, Vol. 18, No. 2, pp. 716~728.

Suh, C. M., Kwon, O. H. and Lee, J. J., 1987b, "Crack Growth Behavior of Fatigue Surface Crack Initiated from a Small Surface Defect," in Korea, *Trans. of KSME*, Vol. 11, No. 2, pp. 191~197.

Suh, C. M., Lee, J. J., Kang, Y. G., Ahn, H. J. and Woo, B. C., 1992, "A Simulation of the Fatigue Crack Process in Type 304 Stainless Steel at 538℃," *Fatigue Fract. Engng Mater. Struct.*, Vol. 15-7, pp. 671~684.

Swain, M. H., 1992, "Monitoring Small-Crack Growth by the Replication Method," ASTM STP 1149, pp. 34~56.

1992, "Standard Test Methods of Tension Testing of Metallic Materials," *Annual Book of ASTM Standards, Part* 10, E8, pp. 130~149.

1992, "Standard Test Method for Measurement of Fatigue Crack Growth Rates," *Annual Book of ASTM Standards*, Part 10, E647, pp. 674~701.